Porous Crystals

Deutsche Ausgabe: DOI: 10.1002/ange.201601807
Internationale Ausgabe: DOI: 10.1002/anie.201601807

Unusually Stable Triazine-based Organic Superstructures

Sun-Min Jung, Dongwook Kim, Dongbin Shin, Javeed Mahmood, Noejung Park, Myoung Soo Lah, Hu Young Jeong, and Jong-Beom Baek**

Abstract: *Solid-state reactions have been rapidly gaining popularity in organic chemistry owing to their simplicity, efficiency, and selectivity compared to liquid-phase reactions. Herein, we describe the formation of superstructures through the solid-state reaction of an organic single-crystal. The superstructure of 5,5′,5″-(1,3,5-triazine-2,4,6-triyl)triisophthalonitrile (TIPN) can be formed by cyclotrimerization of 1,3,5-tricyanobenzene (TCB) single crystals. The TIPN superstructure was confirmed by single crystal X-ray diffraction and visualized by transmission electron microscopy. The superstructure has hexagonally packed 1-dimensional (1D) channels along the crystal axis. Furthermore, the superstructure arises from interdigitated nitrile interactions in the crystal lattice, and thus has electron-beam tolerance and very high thermal stability.*

Merrifield introduced the chemical synthesis of polypeptides by solid-phase reaction in 1963.[1] After his contribution, solid-phase (reactions between solid–liquid or solid–gas phase reactants) and solid-state (the reaction between two solid-phase reactants) organic chemical reactions have rapidly developed, along with improvements in crystal engineering techniques.[2] Solid-state reactions are simple, efficient, and highly selective compared to liquid-phase reactions because the molecules are tightly and regularly orientated in a crystal lattice.[3] The solid-state reactions in modern chemistry involve photochemical reactions,[4,5] thermal reactions,[6] microwave methods,[7] and mechanochemical reactions such as grinding.[8] In addition, Toda introduced host–guest chemistry in solid-state organic reactions towards high selectivity products.[3] Thus, understanding the crystal structure of reactants using X-ray crystallography is a fundamental step for predicting the reactivity of reactants and the structural information of products. This is because the properties of organic solids depend not only on configuration, but also on conformation. The molecular arrangements in organic single crystals can provide clues to how molecules are packed, and allow understanding of the chemical and physical nature of the molecules. Most of the molecular ordering in organic compounds is not driven by chemical reactions, but in response to thermodynamic and statistical parameters crucial for molecular packing in a crystal lattice. Generally, the crystals of organic molecules assemble in response to non-covalent intermolecular interactions such as metal coordination,[9] van der Waals forces,[10–12] π–π interactions,[13] and hydrogen bonding.[14,15] Furthermore, the study of superimposed crystalline structures has been vigorously pursued, with subject areas including ordered supramolecules,[16] metal–organic frameworks (MOFs),[17,18] coordination complexes with particles and polymers,[19] and covalent organic frameworks (COFs).[20,21] However, following the principle of close packing, porous single-crystals resulting from non-covalent interactions are rare because most of the molecules in the solid pack efficiently in ways that minimize the crystal volume.[22] Even so, a few examples have been revealed by X-ray diffraction (XRD), such as the crystal structures of columnar pore channels[5,23] and cage pores.[22,24]

In this work, our strategy was aimed at achieving a solid-state chemical reaction that would yield a well-defined interlocked superstructure. Moreover, this process had to be simple, convenient, and eco-friendly, without the use of organic solvents during synthesis. The new organic compound, 2,4,6-triphenyl-*s*-triazine has C_3 symmetry and six nitrile groups at its periphery. It was realized by a solid-state reaction of 1,3,5-tricyanobenzene single crystals in the presence of hydrochloric acid as a gaseous catalyst. The compound, 5,5′,5″-(1,3,5-triazine-2,4,6-triyl)triisophthalonitrile (TIPN), has not yet been synthesized by conventional synthetic methodology, but for the first time, was created by stagnant cyclotrimerization. The TIPN-formed superstructure was resolved by single-crystal XRD patterns, and its cylindrical channels in the crystal architecture were visualized by transmission electron microscopy (TEM). The TIPN superstructure displayed unusually high thermal stability, owing to six TIPN molecules interlocked to form a hexagonal structure, superimposed by π–π interactions.

Using the synthetic procedure described in Figure 1a, a trifunctional monomer (M3) of 1,3,5-tricyanobenzene (TCB, structure **1**; Figure 1a) was annealed in a sealed glass ampoule at 250 °C in the presence of hydrochloric acid as a gaseous catalyst for the solid-state reaction. Typically, TCB polymerizes into a poly(*s*-triazine) network (CTF-0, structure **3**; Figure 1a) through spontaneous cyclization of three nitrile (−C≡N) groups.[25,26] However, the reaction stagnates after a single cyclotrimerization, producing the TCB trimer, 5,5′,5″-(1,3,5-triazine-2,4,6-triyl)triisophthalonitrile (TIPN, structure **2**; Figure 1a).

[*] S.-M. Jung, Dr. J. Mahmood, Prof. Dr. J.-B. Baek
School of Energy and Chemical Engineering
Center for Dimension Controllable Organic Frameworks
Ulsan National Institute of Science and Technology (UNIST)
50 UNIST, Ulsan 44919 (Korea)
E-mail: jbbaek@unist.ac.kr
D. Kim, Prof. Dr. M. S. Lah
Department of Chemistry, UNIST (Korea)
D. Shin, Prof. Dr. N. Park
Department of Physics, UNIST (Korea)
Prof. Dr. H. Y. Jeong
UNIST Central Research Facilities (UCRF), UNIST (Korea)
E-mail: hulex@unist.ac.kr

Supporting information for this article can be found under: http://dx.doi.org/10.1002/anie.201601807.

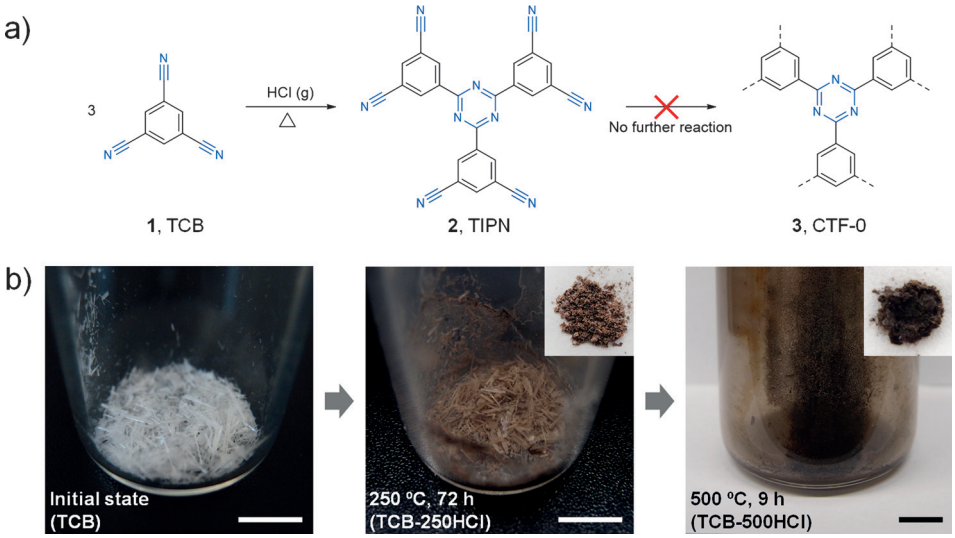

Figure 1. a) Representation of TIPN formation after a single cyclotrimerization of TCB single-crystals. b) Digital photographs of TCB at different temperatures and times showing the progress of the solid-state reaction. The color change of the sample, from white to light brown, suggested that the solid-state reaction occurred at 250 °C (below TCB melting temperature) in the presence of dry gaseous HCl. After further heat-treatment at 500 °C, the color of the sample changed to dark brown. The scale bars indicate 1 cm. The inset images are the final products on weighing paper after work-up.

For the above solid-state reaction, TCB was recrystallized from ethanol to grow rod-shaped monoclinic crystals by rich π–π interactions (Supporting Information, Figure S1a), and its structure was revealed by single-crystal XRD (Figures S2, S3 and Table S1). On the basis of crystallographic information, we recognized that nitrile groups in TCB crystals interacted with three adjacent molecules having average distance of 3.88 Å (each distance between carbon and nitrogen: 3.56 Å; 3.28 Å; 4.31 Å; Figure S2b). The distance among nitrile groups is within the range of cyclotrimerization. However, high energy (high pressure and temperature above melting) was required to drive the formation of *s*-triazine rings.[27] On the other hand, the solid-state reaction must occur below the melting temperature of the reactants. Differential scanning calorimetry (DSC) indicated that the melting temperature of TCB is 260 °C (Figure S4), but the temperature of cyclotrimerization of nitrile groups is typically above 300 °C. Acid catalysts may play an important role for the formation of *s*-triazine from three nitrile groups of TCB under much milder conditions (Figure S5).[28,29] Still, the acid-catalyzed cyclotrimerization of TCB required a liquid-phase reaction in solution and/or a molten state.

For the solid-state reaction, we chose dry gaseous hydrogen chloride (HCl) as a catalyst for the following reasons: 1) to efficiently remove catalyst during work-up procedures; 2) to avoid use of solvents for green chemistry; and 3) to minimize the formation of by-products, such as conversion of nitrile into carboxylic acid in the presence of acid and moisture. To identify the role of HCl, control reactions were carried out with and without the presence of HCl at 250 °C (samples denoted as TCB-250HCl and TCB-250, respectively). In the case of TCB-250, no reaction occurred, as evidenced by Fourier transform infrared spectroscopy (FT-IR; Figure S6). The negligible peak intensities of *s*-triazine from TCB-250 were observed at both 1531 and 1360 cm^{-1}. They are almost identical to those of the starting TCB. On the other hand, TCB-250HCl showed strong *s*-triazine peaks, suggesting that only thermal annealing TCB at 250 °C in the presence of HCl can induce the formation of *s*-triazine in solid-state (Figure S6 and S7). However, the yield of TCB-250HCl was low (≈6 %). We speculated that the yield was low because only the exposed surface of the TCB single crystals had contact with the HCl catalyst and cyclized to form *s*-triazine. As described in the detailed illustrations of the single crystal structure of TCB (Figure S2), TCB molecules at the surface have more freedom of motion before melting. The mechanism for cyclotrimerization causes the TCB molecules to first form α-halogenated alkyl cyanides with HCl, and then to cyclize into *s*-triazine rings in solid-state.[29] Therefore, preformed triazine frameworks were stable enough for further heat-treatment at 500 °C, which greatly increased yield (21.3 %, sample denoted as TCB-500HCl; Figure 1 b). After incrementally increasing the reaction temperature to 500 °C, the crystal morphology still remained (Figure S1c), indicating the stability of the products.

The structure of the resultant TCB-500HCl was determined by single-crystal XRD (Figures 2, S8, S9 and Table S2). TCB-500HCl turned out to be TIPN, which has monoclinic crystal structure with space group *C*12/c1. The crystal packing structure shows that the TIPN molecules are aligned along the crystallographic *b*-axis with a 26° tilt from the crystallographic *ac*-plane (Figure 2 a), and are interdigitated to form a one-dimensional (1D) zigzag ribbon structure (Figures 2, S8c and S8d). The molecules aligned along the crystallographic *b*-axis are π–π stacked to form a 1D column (Figures 2 a and S8e). The combination of interdigitation and π–π stacking leads to corrugated 2D sheets, which form a series of 1D solvent channels of 6.5 Å diameter along the crystallographic *b*-axis in a crystallographic two-fold symmetry (Figure 2 a). The crystal channel maintained itself without guest solvent, however, a trace of moisture (0.17 mol %) was contained in the vacant channels of TIPN (Figure S8b and Table S2). Additionally, the powder XRD pattern supported proof of uniformity in the bulk of TIPN (Figure S9). Regarding the poly(*s*-triazine) network, CFT-0, which is synthesized by ionothermal reaction from TCB in the presence of zinc chloride ($ZnCl_2$) as a catalyst,[25] there were no clear XRD patterns observed like those of TIPN crystal in this study. Thus, the powder XRD patterns shown in Figure S9 are a unique feature of TIPN single crystals. This result, in turn, implies that stagnant cyclotrimerization of TCB had occurred

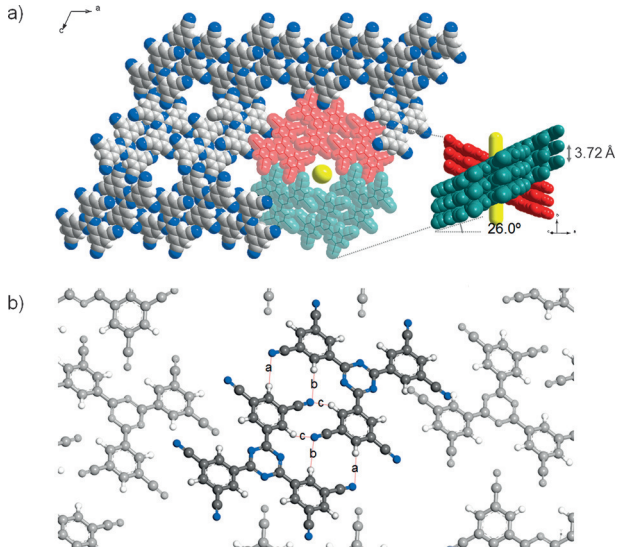

Figure 2. a) Diagram of TIPN viewed along the crystallographic *b*-axis. The yellow ball and stick represent traces of water at partial occupancy sites in the solvent channels (color codes: grey = carbon; blue = nitrogen; white = hydrogen). b) Ball-and-stick packing diagram of TIPN crystal and red lines indicate interdigitation between two TIPNs by dipole–dipole interactions with each distance; a: 2.75 Å; b: 2.76 Å, and c: 2.71 Å.

rather than subsequent extension into a CTF-0 network polymer in solid-state.

Density functional theory (DFT) calculations were performed to understand how tightly TIPN molecules are packed in the crystal lattice, and why subsequent polymerization of TCB ceased after formation of a single *s*-triazine into TIPN. The formation energy of a single *s*-triazine ring from three TCBs was computed to be −2.84 eV, and that of a triazine-based network polymer (CTF-0) was computed to be −2.86 eV, for the sequential formation of *s*-triazine rings (Figure S10). The thermodynamic energy requirement is similar for formation of a single *s*-triazine ring from TIPN and CTF-0. However, the TIPN molecules forming in the crystal lattice are thermodynamically much more stable than individual TIPN molecules (Figure S11a) because they are interlocked by strong dipole–dipole interactions (−C−H···N≡C−) of −1.49 eV between two TIPN molecules. They are stacked tightly by van der Waals force of −1.41 eV (Figure S11a), which is a much more stable and favorable state than that of TCB (Figure S11b). Because the TIPN molecules are tightly bound in the stable crystal structure (Figure 2b), they cannot extend the structure as a network polymer, CTF-0, even after annealing at 500 °C.

The morphology and crystal facets (Figure 3a) of TIPN were studied using scanning electron (SEM) and transmission electron (TEM) microscopy, respectively. Figures 3b and S12 show that TIPN crystals are long 1D wires with a width of approximately 1–2 μm. Significantly longer wires (> 100 μm) were also observed (Figure S12c). SEM energy-dispersive spectroscopy (EDS) indicated that TIPN consisted of carbon and nitrogen with little physically absorbed oxygen (Figure S13). The selected-area electron diffraction (SAED) pattern from the TIPN 1D wire (Figure 3c), which was mounted on a carbon-coated copper grid, displayed a single-crystal diffraction with high crystallinity. The growth direction was parallel to [010] (crystallographic *b*-axis of unit cell). A magnified SEM image (inset, Figure 3b) showed that the surface of a TIPN crystal was multi-faceted. To clearly investigate the cross-sectional shape of TIPN crystals, we fabricated a cross-sectioned TEM sample using a focused ion beam (FIB; Figure S14). The bright-field (BF) TEM image of the cross-section of the TIPN crystal indicated a hexagonal type (Figures 3e and S15a), while others of octagonal shape

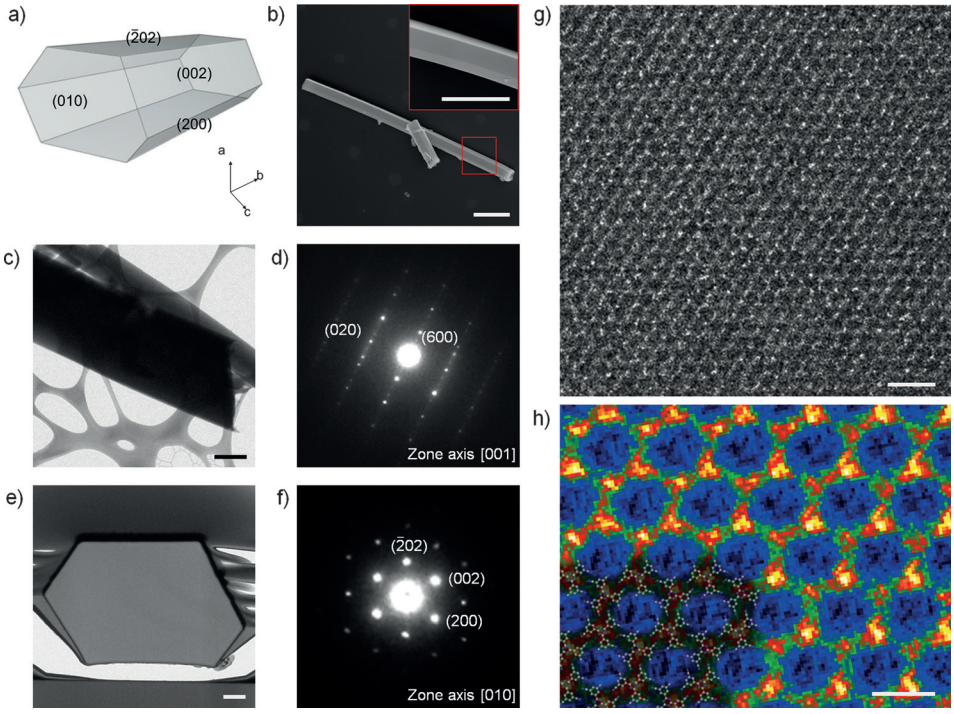

Figure 3. a) Diagram of TIPN crystal facets revealed by TEM; b) SEM images of TIPN crystal: Inset is the magnified image from red square. c) TEM images of TIPN. d) Selected area electron diffraction (SAED) pattern from (c) region. The crystal (001) facet is parallel to the grid. e) Cross-sectional TEM image of TIPN crystal prepared by FIB. f) SAED pattern from (e) region depicting zone axis of [010]. The main crystal growth direction is perpendicular to the image plane, the crystallographic *b*-axis. g) Atomic-resolution TEM image of the magnified region in (e), which shows a well-ordered crystal lattice. h) Inverse fast-Fourier transform (IFFT) image. The image is matched with a TIPN crystallographic model determined by XRD (color codes: grey = carbon; blue = nitrogen). Scale bars: b) 5 μm; c) 500 nm; e) 200 nm; g) 5 nm; h) 2 nm.

were observed (Figure S15c). The major cross-section was the hexagonal type (≈78.5%), which may be related to surface energy minimization (Figure S16). For assigning crystal facets, it was also noted that the SAED pattern (Figure 3f) from the cross-section samples was well matched with the simulated electron diffraction (ED) pattern (Figure S17b) of the above-mentioned monoclinic crystal structure, which was viewed along the [010] direction. The hexagonal surface facets were mainly composed of (−202), (002), and (200) planes (Figure 3a). It is challenging to observe high-resolution TEM (HR-TEM) images of the pores of organic materials because they are easily damaged by strong electron beam irradiation or require special conditions, such as cryogenic temperature.[30] However, the TIPN crystals were robust enough to endure an electron beam operated at 80 kV. As a result, we were able to obtain the HR-TEM cross-section images shown in Figures 3g and S18a, which show well-ordered quasi-molecular frameworks. Furthermore, the inverse fast-Fourier transform (IFFT) image (Figure 3h) clearly visualized the channel, which was described by a crystallographic atomic TIPN model (Figure 2). This result is in good agreement with a simulated HR-TEM image confirming the existence of columnar channels (Figure S17c). The bond nature and the qualitative analysis by electron energy loss spectroscopy (EELS) suggest that TIPN consists of carbon and nitrogen atoms (Figure S19).

Spectroscopic analyses were also carried out to provide additional information about the structure of TIPN. The ionized molecular mass of TIPN by electron ionization mass spectroscopy (EI-MS) precisely matched with the calculated values (Figure S20). In addition, the bond nature of TIPN was further determined using Fourier transform infra-red (FT-IR) spectroscopy, indicating that *s*-triazine rings show strong peaks at both 1545 and 1372 cm^{-1} (Figure S21a).[31] As expected from the crystal lattice information (Figure 2) and DFT calculations (Figure S11a), TIPN crystals have high stability. Indeed, TIPN crystals showed unusually high thermal stability (Figure S21b) owing to their planar structure, and each nitrile group tightly interlocked with other nitrile groups in the crystal lattice. The maximum decomposition temperature was as high as 605 °C in nitrogen gas, which was more stable than TCB (326 °C, Figure S21b). After heating to 1000 °C, the char yield was 5.8% (inset, Figure S21b).

To determine details of the 1D inner channel of TIPN crystals, gas absorption/desorption were carried out using Brunauer–Emmett–Teller (BET) measurements. The cavity volume was 15.3% in TIPN crystals, which was calculated using PLATON software (the accessible volume by a 1.2 Å probe and the cell volume). Thus, we could confirm the presence of a cavity in TIPN, which adsorbed nitrogen gas (up to 17.26 $cm^3 g^{-1}$) at 77 K and carbon dioxide to 12.73 $cm^3 g^{-1}$ at 196 K and 0.96 bar, showing typical micropore isotherms (Figure S21c). In the cylindrical channel, TIPN adsorbed CO_2 better at < 0.9 bar than N_2. This is because CO_2 is slightly thinner than N_2, even if they are both linear molecules, and because there are electrostatic interactions between a surface with abundant π-electrons and the CO_2 molecule.[32] The BET surface area calculated from CO_2 adsorption was 41.50 $m^2 g^{-1}$ at 196 K with a pore volume of 7.15 $cm^3 g^{-1}$. Although the calculated BET surface area and gas adsorption amount are relatively low owing to the narrow channel diameter (≈6.5 Å), we confirmed a channel cavity.

In summary, the superstructure of TIPN was, for the first time, realized using stagnate cyclotrimerization of TCB single crystals in solid-state. The formation of TIPN superstructure was confirmed by single-crystal XRD and visualized by TEM, confirming that hexagonally packed TIPN molecules with C_3 symmetry and six nitrile groups interlocked into a 1-dimensional rod with concentric hollow channels. The TIPN superstructure displayed unusually high thermal stability and electron-beam tolerance owing to interdigitated TIPN molecules forming a quasi-molecular framework. The formation of TIPN-based robust superstructure may open up a new class of stable organic frameworks. Thus, this class of stable molecular frameworks will be useful for many applications, ranging from wet chemistry to specific devices.

Acknowledgements

This work was supported by the Creative Research Initiative (CRI) and BK21 Plus programs through the National Research Foundation (NRF) of Korea.

Keywords: interdigitation · porous organic crystals · single-crystals · solid-state reactions · superstructures

How to cite: *Angew. Chem. Int. Ed.* **2016**, *55*, 7413–7417
Angew. Chem. **2016**, *128*, 7539–7543

[1] R. B. Merrifield, *J. Am. Chem. Soc.* **1963**, *85*, 2149–2154.
[2] G. Rothenberg, A. P. Downie, C. L. Raston, J. L. Scott, *J. Am. Chem. Soc.* **2001**, *123*, 8701–8708.
[3] F. Toda, *Acc. Chem. Res.* **1995**, *28*, 480–486.
[4] V. Ramamurthy, K. Venkatesan, *Chem. Rev.* **1987**, *87*, 433–481.
[5] M. Baroncini, S. O'Agostino, G. Bergamini, P. Ceroni, A. Comotti, P. Sozzani, I. Bassanetti, F. Grepioni, T. M. Hernandez, S. Silvi, M. Venturi, A. Credi, *Nat. Chem.* **2015**, *7*, 634–640.
[6] I. C. Paul, D. Y. Curtin, *Acc. Chem. Res.* **1973**, *6*, 217–225.
[7] R. B. N. Baig, R. S. Varma, *Chem. Soc. Rev.* **2012**, *41*, 1559–1584.
[8] B. P. Biswal, S. Chandra, S. Kandambeth, B. Lukose, T. Heine, R. Banerjee, *J. Am. Chem. Soc.* **2013**, *135*, 5328–5331.
[9] J. S. Seo, D. Whang, H. Lee, S. I. Jun, J. Oh, Y. J. Jeon, K. Kim, *Nature* **2000**, *404*, 982–986.
[10] P. Sozzani, S. Bracco, A. Comotti, L. Ferretti, R. Simonutti, *Angew. Chem. Int. Ed.* **2005**, *44*, 1816–1820; *Angew. Chem.* **2005**, *117*, 1850–1854.
[11] V. Z. Yu, P. M. Zorkii, *Russ. Chem. Rev.* **1989**, *58*, 421.
[12] G. D. Enright, K. A. Udachin, I. L. Moudrakovski, J. A. Ripmeester, *J. Am. Chem. Soc.* **2003**, *125*, 9896–9897.
[13] M. Watanabe, Y. J. Chang, S. W. Liu, T. H. Chao, K. Goto, M. M. Islam, C. H. Yuan, Y. T. Tao, T. Shinmyozu, T. J. Chow, *Nat. Chem.* **2012**, *4*, 574–578.
[14] G. R. Desiraju, *Acc. Chem. Res.* **1991**, *24*, 290–296.
[15] G. R. Desiraju, *Angew. Chem. Int. Ed.* **1995**, *34*, 2311–2327; *Angew. Chem.* **1995**, *107*, 2541–2558.
[16] L. C. Gilday, S. W. Robinson, T. A. Barendt, M. J. Langton, B. R. Mullaney, P. D. Beer, *Chem. Rev.* **2015**, *115*, 7118–7195.
[17] H. Li, M. Eddaoudi, M. O'Keeffe, O. M. Yaghi, *Nature* **1999**, *402*, 276–279.

[18] S. Furukawa, J. Reboul, S. Diring, K. Sumida, S. Kitagawa, *Chem. Soc. Rev.* **2014**, *43*, 5700 – 5734.
[19] N. Belman, J. N. Israelachvili, Y. Li, C. R. Safinya, V. Ezersky, A. Rabkin, O. Sima, Y. Golan, *Phys. Chem. Chem. Phys.* **2011**, *13*, 4974 – 4979.
[20] A. P. Côté, A. I. Benin, N. W. Ockwig, M. O'Keeffe, A. J. Matzger, O. M. Yaghi, *Science* **2005**, *310*, 1166 – 1170.
[21] X. Feng, X. Ding, D. Jiang, *Chem. Soc. Rev.* **2012**, *41*, 6010 – 6022.
[22] T. Tozawa, J. T. A. Jones, S. I. Swamy, S. Jiang, D. J. Adams, S. Shakespeare, R. Clowes, D. Bradshaw, T. Hasell, S. Y. Chong, C. Tang, S. Thompson, J. Parker, A. Trewin, J. Bacsa, A. M. Z. Slawin, A. Steiner, A. I. Cooper, *Nat. Mater.* **2009**, *8*, 973 – 978.
[23] I. Hisaki, H. Senga, H. Shigemitsu, N. Tohnai, M. Miyata, *Chem. Eur. J.* **2011**, *17*, 14348 – 14353.
[24] T. Mitra, X. Wu, R. Clowes, J. T. A. Jones, K. E. Jelfs, D. J. Adams, A. Trewin, J. Bacsa, A. Steiner, A. I. Cooper, *Chem. Eur. J.* **2011**, *17*, 10235 – 10240.
[25] P. Katekomol, J. Roeser, M. Bojdys, J. Weber, A. Thomas, *Chem. Mater.* **2013**, *25*, 1542 – 1548.
[26] L. Hao, J. Ning, B. Luo, B. Wang, Y. Zhang, Z. Tang, J. Yang, A. Thomas, L. Zhi, *J. Am. Chem. Soc.* **2015**, *137*, 219 – 225.
[27] I. S. Bengelsdorf, *J. Am. Chem. Soc.* **1958**, *80*, 1442 – 1444.
[28] L. E. Hinkel, R. T. Dunn, *J. Chem. Soc.* **1930**, 1834.
[29] C. Grundmann, A. Kreutzberger, *J. Am. Chem. Soc.* **1954**, *76*, 5646 – 5650.
[30] P. Kissel, R. Erni, W. B. Schweizer, M. D. Rossell, B. T. King, T. Bauer, S. Gotzinger, A. D. Schluter, J. Sakamoto, *Nat. Chem.* **2012**, *4*, 287 – 291.
[31] P. Kuhn, M. Antonietti, A. Thomas, *Angew. Chem. Int. Ed.* **2008**, *47*, 3450 – 3453; *Angew. Chem.* **2008**, *120*, 3499 – 3502.
[32] I. Hisaki, S. Nakagawa, N. Tohnai, M. Miyata, *Angew. Chem. Int. Ed.* **2015**, *54*, 3008 – 3012; *Angew. Chem.* **2015**, *127*, 3051 – 3055.

Received: February 21, 2016
Revised: April 4, 2016
Published online: April 27, 2016

